High Power Laser Science and Engineering, (2025), Vol. 13, e4, 7 pages.
doi:10.1017/hpl.2024.84

HIGH POWER LASER SCIENCE AND ENGINEERING

RESEARCH ARTICLE

Coherent combining of large-aperture high-energy Nd:glass laser amplifiers

Pierre Lebegue[1,2], Joanna De Sousa[2], Cyril Rapenau[2], Doina Badarau[2], Jordan Andrieu[2], Patrick Audebert[2], Frédéric Druon[1], and Dimitrios Papadopoulos[2]

[1] *Université Paris-Saclay, Institut d'Optique Graduate School, CNRS, Laboratoire Charles Fabry, Palaiseau, France*

[2] *Laboratoire pour l'Utilisation des Lasers Intenses, Laboratoire Charles Fabry, CNRS, Ecole Polytechnique, Palaiseau, France*

(Received 26 July 2024; revised 4 November 2024; accepted 13 November 2024)

Abstract

We present coherent beam combining of nanosecond pulses with 20-J energy and large beams using a Sagnac interferometer geometry based on Nd:glass rod-type amplifiers. In this study, we demonstrate that coherent beam combining is compatible with large-diameter energetic beams, presenting, therefore, an interesting and solid perspective towards the performance improvement of large-scale laser facilities, especially in terms of high-repetition-rate and high-energy operation. We demonstrate that for energy of 20 J, the coherent combination efficiency is around 92%, with high beam quality and long-term stability. A thorough temporal and spatial characterization of the system's operation is provided to forecast the various potentialities available for large-scale facilities.

Keywords: high energy; coherent beam combining; nanosecond; large aperture; Nd:glass

1. Introduction

In recent years, high-energy lasers (multi-hundred joule class) have attracted the interest of the international community, notably with the first results from controlled-gain inertial confinement fusion[1], but also as scientific research tools, for example in plasma physics and in various laser-based material processing methods such as shock-peening[2]. However, all these applications currently suffer from the low repetition rate of such lasers, typically ranging from several minutes to several hours between shots. To reach the kJ-class operation level, end chain amplification stages employ active media of several tens of centimeters in diameter, which apart from the technological complication for their fabrication and their cost, present low cooling efficiencies, imposing long times between successive shots. One possible solution to this limitation is coherent beam combining (CBC). This technique is based on the parallelization of the amplification using several smaller apertures and, therefore, higher repetition rate amplifiers whose output beams are subsequently coherently recombined. CBC has already been successfully applied, mostly for low-energy systems in the mJ range. Several CBC architectures, passive or active, temporal or spatial[3], have proven their potential for fiber system[4,5] and bulk mJ-range systems[6–8]. Up to now, the experimental demonstrations involve small-size beams where the spatial homogeneity has not been an issue, reducing the phasing problem to a single dimension and the temporal delay control. These lasers, operating in general at high repetition rates[8,9], give access to adequate feedback loops operating in the kHz regime. Furthermore, in such systems the amplification regime is in the steady state with respect to the gain dynamics, without strong shot-to-shot phase variations. In a different context restricted to high-energy nanosecond narrow linewidth lasers, nonlinear processes such as stimulated Brillouin scattering (SBS) can also be used[10–12] to perform CBC. The spatial effects, in this case, are addressed using a nonlinear amplification process that transfers energy from pump beams to a signal beam. However, SBS-based CBC architectures are not compatible with broadband sources and are very demanding in terms of the short- and long-term stability of the individual sources[13]. In this context, efficient CBC at high energy and low repetition rate remains to be demonstrated, with questions related to the individual source wavefront aberrations and potential unpredictable shot-to-shot phase instabilities.

Correspondence to: D. Papadopoulos, Laboratoire pour l'Utilisation des Lasers Intenses, Laboratoire Charles Fabry, CNRS, Ecole Polytechnique, 91128 Palaiseau, France. Email: dimitrios.papadopoulos@polytechnique.edu

To this end, we demonstrate a proof-of-concept CBC experiment based on a robust, easy-to-implement architecture using amplifiers embedded in a Sagnac interferometer geometry[14], with multi-cm aperture bulk Nd:glass gain media. This passive CBC implementation requires no servo-control loops, which is particularly adapted to low-repetition-rate systems. It is based solely on polarization separation and recombination and is directly compatible with already-existing high-energy laser chains. The input pulse is first split into two orthogonally polarized beams, each carrying half of the energy. Each beam is amplified separately, thereby reducing the fluence on the amplifier media and minimizing nonlinear effects such as the B-integral. As a beneficial outcome, this enables us to operate further away from the damage threshold or equivalently to reduce the diameter of the amplifiers from the perspective of potentially increasing the repetition rates. Once the two beams are amplified, they are combined in phase to form a single beam. In the Sagnac interferometer, the two counter-propagating pulses automatically share the same optical path, leading to a particularly robust operation against air turbulence or mechanical vibrations in the two amplifying arms of the setup.

2. Setup

In this work, we study the performance of the coherent combination of high-energy large beams by varying different parameters, such as the input energy, as well as the shape and the duration of the pulses. To achieve this objective and validate the potential of the technique in the frame of already operating systems, the CBC experiment is performed at an existing nanosecond high-energy Nd:glass laser facility named HERA-LULI. This facility is based on flash-lamp pumped Nd-phosphate amplifiers, and can deliver pulses at the 100 J level. The CBC experiment focuses on the pre-amplifiers of the chain, which produce pulses at the 10 J level. The front-end of these amplifiers is based on an all-fiber master oscillator power amplifier (MOPA) seeder system and a semiconductor optical amplifier (SOA)[15] that allows active temporal shaping for pulse durations ranging from 3 to 20 ns with sub-nanosecond modulation speed. The pulses are then amplified up to few millijoules with a neodymium-doped yttrium lithium fluoride (Nd:YLF) regenerative amplifier before passing through two 16-mm diameter Nd:glass amplifiers, followed by another two 25-mm diameter amplifiers (Figure 1). Throughout the experiment, we keep the flash voltages of all the amplifiers constant, varying only the regenerative amplifier's output energy to obtain between 200 mJ and 2.7 J in the input of our Sagnac interferometer. The pre-amplification stages are protected from any potential retro-injected light by two Faraday isolators and a Pockels cell isolator.

The Sagnac interferometer includes two flash-pumped amplifier rods of 45 mm in diameter and 250 mm in length, made of Nd:phosphate-glass (1% doped N31 glass with typical optical quality better than λ/8 PV and λ/30 RMS). The small signal gain of each amplifier is around 10, and the stored energy is estimated to be approximately equal to 50 J. The input beam (with a diameter of 38 mm to avoid diffraction at the edges of the rods) enters the Sagnac

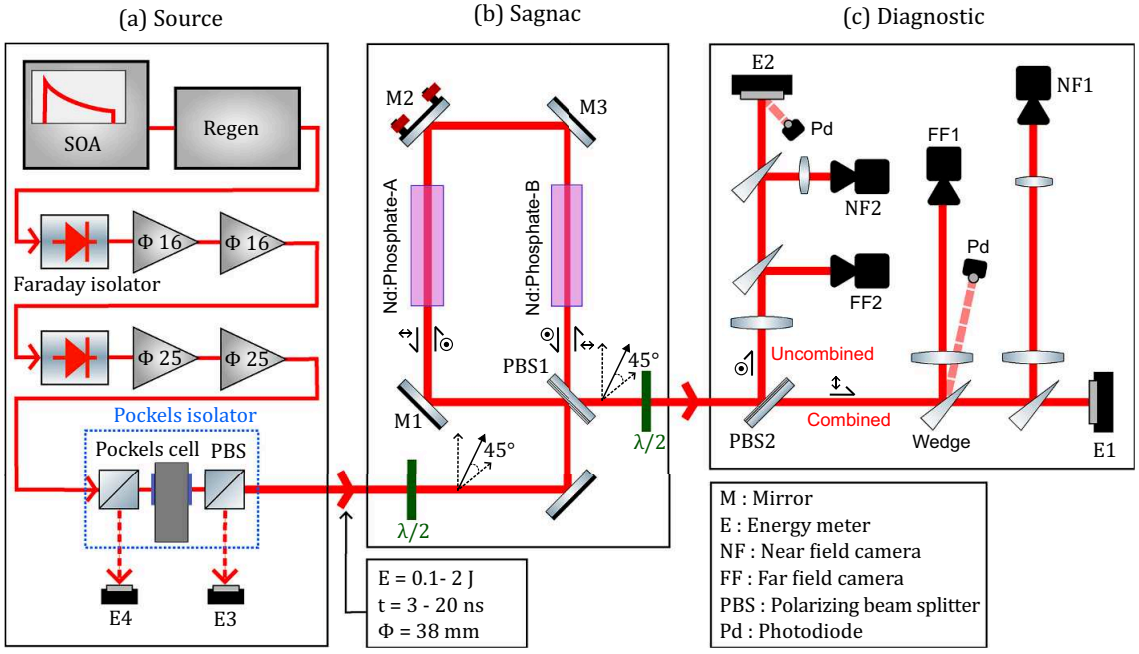

Figure 1. Schematic of the experimental setup: (a) laser source and pre-amplifiers of the HERA laser facility; (b) Sagnac interferometer used for parallel amplification and coherent combining; (c) diagnostics for energetic, spatial and temporal single-shot analysis of the combined and the uncombined beams.

https://doi.org/10.1017/hpl.2024.84 Published online by Cambridge University Press

loop polarized at 45° and is split by a thin film polarizer (PBS1) in two orthogonally polarized equal halves. The two beams propagate in the Sagnac interferometer in counter-propagating paths (anti-clockwise for the S-polarized beam and clockwise for the P-polarized beam) before arriving back on PBS1, where the S-polarized part is transmitted, and the P-polarized part is reflected and coherently combined. Depending on the alignment precision of the Sagnac interferometer, the two polarization components can be combined with their initial phase relation, resulting in a perfectly linearly polarized single beam at 45°. However, the collinearity imperfections, as well as all other phase differences over the full aperture of the beam, can result in deviations from this ideal case and alter the polarization state of the output beam. In our setup, we use mirror M2 (Figure 1) equipped with pico-motors to align the Sagnac interferometer to ensure the same optical path for the P and S waves, thus bringing them with the same phase on the output polarizer. At the output of the Sagnac interferometer, we use a half-wave plate and a second identical polarizing plate (PBS2) in order to separate the two orthogonally polarized beams. In the ideal case, the transmitted light carries all the energy (noted as combined output). Any residual phase error in the Sagnac interferometer results in the observation of light in the orthogonal polarization state, the uncombined output. The diagnostics of the output beam (Figure 1) are designed to simultaneously perform single-shot acquisitions of the energies, the temporal profiles and the near-field and far-field spatial profiles for both combined and uncombined beams.

3. Alignment procedure

The M2 mirror of the interferometer allows the precise adjustment of the beam angles in the horizontal and vertical planes, respectively, α and β. A variation in β deflects the P and S beams in the same direction with no impact on their collinearity but induces a non-negligible delay between the two pulses due to an effective difference in the propagation path of each beam in the PBS1 substrate. A variation of α deflects the P and S beams in opposite directions, producing a relative horizontal tilt between these two beams. Both α and β are controlled with an angular resolution of 0.7 µrad provided by the motorized mirror mount (Newport^{TM} ref 8824-AC). Such resolution allows us to control the relative tilt, adjusting the α angle, with an accuracy of $\lambda/40$, and the relative delay using the β angle, with an accuracy better than $\lambda/100$. Figure 2 shows the progressive adjustment of α until only one interference fringe is observed. Adjusting the angle β permits the switching of the combined and uncombined channels. The alignment is first done to minimize the uncombined beam energy without amplification at 10 Hz repetition rate. However, due to a systematic on-shot phase offset in the amplifiers in the Sagnac interferometer, we had to apply a small systematic angular offset of $\alpha \approx 6$ µrad and $\beta \approx 77$ µrad in order to obtain the best combination upon amplification. This effect is under investigation and could be attributed to the geometry of the rods and/or to gain profile asymmetries between the two amplifiers. However, this offset remained the same for all the shots realized in this experiment.

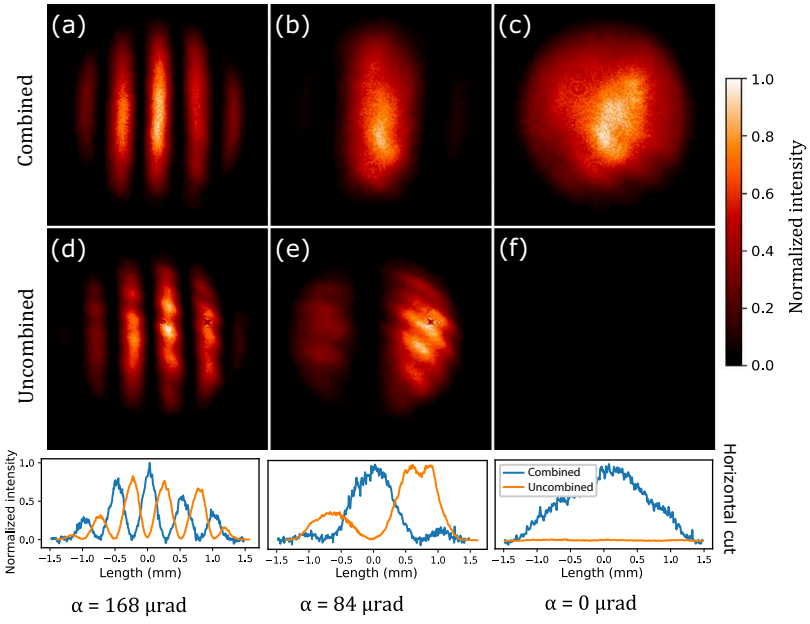

Figure 2. Near-field profiles at low energy through the alignment procedure at 10 Hz: (a)–(c) images show the profiles of the combined channel, while (d)–(f) images show those of the uncombined channel. Each column represents an acquisition with a progressively smaller α misalignment angle (α = 168, 84 and 0 µrad) converging to 0. Each image is normalized to have a scale consistent with its energy.

https://doi.org/10.1017/hpl.2024.84 Published online by Cambridge University Press

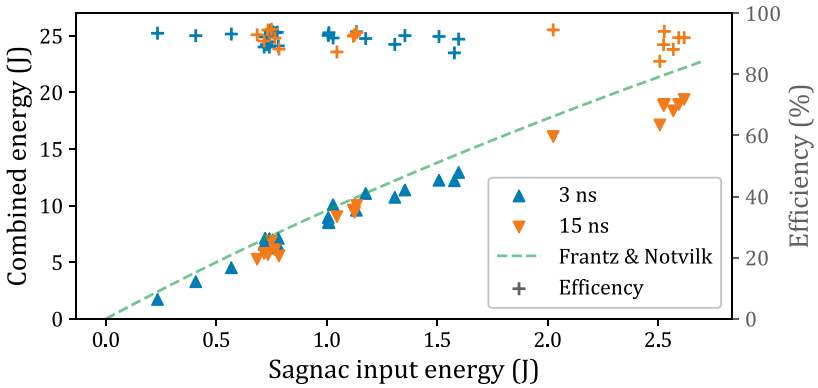

Figure 3. Combined output energy and combining efficiency as a function of Sagnac interferometer input energy. Measurements are taken for pulses durations of 3 ns (blue) and 15 ns (orange), respectively. The total-energy amplification curve follows the Frantz–Nodvik model (dashed green line).

Firstly, we vary the input pulse energy in the Sagnac interferometer from 0.2 to 2.7 J. The input energy is limited so that we do not exceed the nominal operation point, that is, 10 J per amplifier. The combining efficiency in our experiment is defined by $\eta = E_C/(E_C + E_U + E_B)$, where E_C is the combined energy, E_U is the uncombined energy and E_B is the energy of the backward beam, which is measured with energy meters E3 and E4 (Figure 1). The retro-injected light could be generated from depolarization effects in the Nd:glass rods or imperfections of PBS1. However, with more than 200 shots during our entire campaign, the retro-injected energy never exceeded 0.1% of the total energy. This is a very critical point to consider regarding the system security since a backward beam could damage the front-end, and we demonstrate it is negligible. To simplify, we can, therefore, consider that the combination efficiency depends mainly on the differential wavefront between the P and S beams: $\eta \approx E_C/(E_C + E_U)$. It is useful to note that for applications where the polarization is not an issue, the polarizing-plate analyzer (PBS2) is not required, and 99.9% of the amplifier energy is carried by a single beam that can be effectively used on a target. Output energies and the corresponding combining efficiencies are plotted in Figure 3 as a function of the input energy. We observe a very robust operation of the interferometer with an average combination efficiency of 92%, reaching up to 95%. For comparison, we also plot (dashed green line) the predicted total output energy for perfect combination based on a one-dimensional (1D) Frantz–Nodvik model (assuming a small signal gain $G_0 = 10.5$ and saturation fluence $J_{sat} = 4.2$ J/cm²), showing a very good agreement with the total output energy $E_C + E_U$ (not represented in the graph).

4. Results and discussion

We also studied the influence of the pulse duration on CBC for pulse durations of 15 and 3 ns. For the length of our Sagnac interferometer (about 1 m between the two amplifiers), the 3-ns-duration pulses do not overlap in the amplifiers, whereas for 15 ns there is a partial temporal overlap. Figure 3 shows that this pulse overlap has no impact on the combining efficiency. Indeed, the cross-polarization of the two beams prevents the appearance of any 'spatial hole burning' effect. The measurement presented in Figure 3 took a total of 6 hours over two different days, showing the interferometer's long-term stability.

Figure 4 shows the spatial profiles resulting from CBC for the highest energy. The energy contained on the combined channel represents 92% of the total energy (Figure 4(a)). The rest appears on the uncombined channel (Figure 4(b)), where we can clearly see that combination defects occur mainly on the periphery of the beam. We note that the diagnostics of the uncombined beam are not perfectly optimized, resulting in some beam clipping on the mount of PBS2 causing the observed concentric fringes. The presence of a 'dip' in the middle of the combined beam is due to doping inhomogeneity and is present when the amplifiers operate in CBC mode or independently (Figure 4(d)). No difference between the CBC and the independent operation mode can be distinguished. The far field of the combined beam is shown in Figure 4(c) and the aberrations are mostly due to the imaging system. To conclude, this CBC architecture preserves all the spatial performances of the amplifiers compared to a conventional laser chain.

In addition, two sets of experiments have been performed to demonstrate the compatibility of the CBC system with the temporal shaping requirements. Firstly, we can see in Figure 5 that the combined and uncombined channels are rather consistent in terms of fluctuations and that the combining efficiency over time, $\eta(t)$, decreases only slightly by 2% during the pulse. This indicates that coherent combination occurs continuously and homogeneously throughout the pulse duration. Two typical temporal pulse shapes are explored in our experiments: a square input shape at the input of the regenerative amplifier (Figure 5) without saturation pre-compensation resulting in a 'triangular' shape at the output, and a shape that is pre-compensated for saturation

https://doi.org/10.1017/hpl.2024.84 Published online by Cambridge University Press

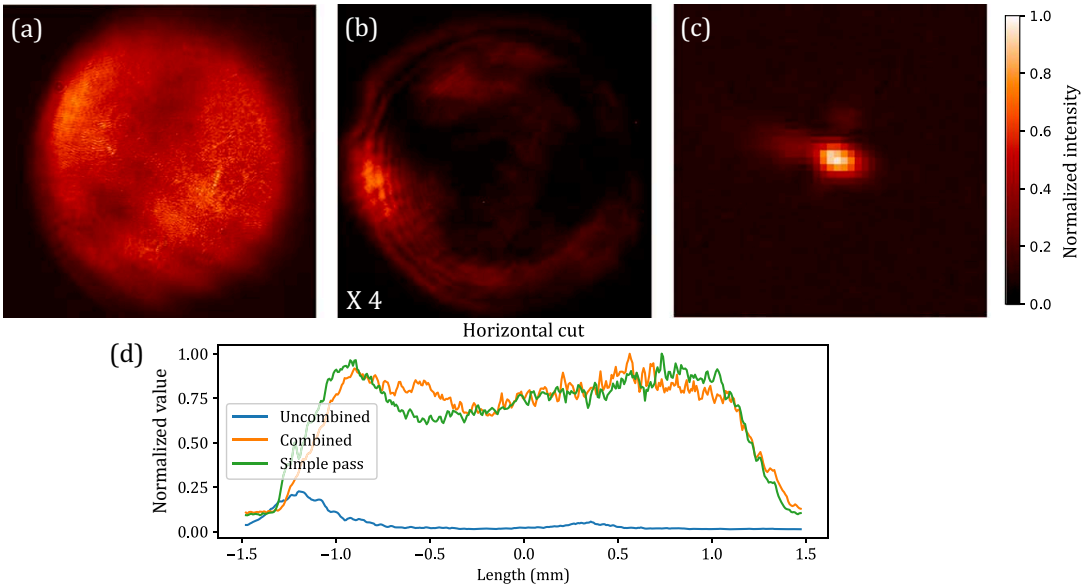

Figure 4. Spatial profiles of the Sagnac interferometer output beam: (a) near field of the combined beam; (b) near field of the uncombined beam; (c) far field of the combined beam; (d) horizontal cut of (a) and (b) compared to the reference beam without CBC. The profiles shown in (a)–(c) have been obtained simultaneously with the highest energy (21.1 J, $\eta = 92\%$).

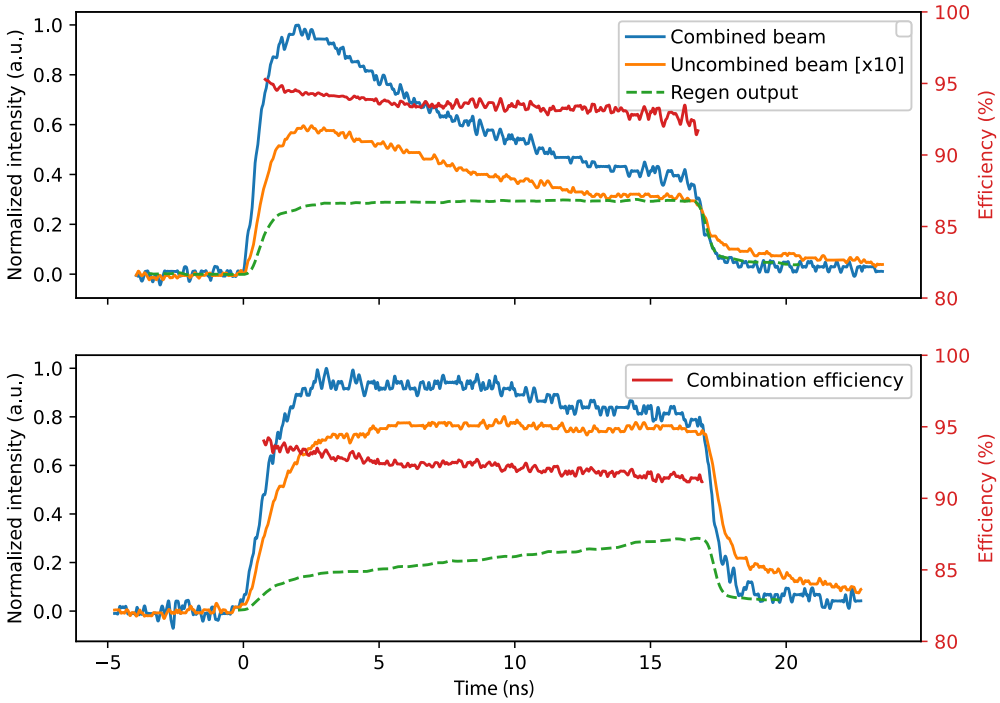

Figure 5. Temporal profiles of the input pulse just after the regenerative amplifier (green line not to scale for better visibility), the combined pulse (blue) and the uncombined pulse (orange line). The instantaneous combining efficiency $\eta(t)$ is plotted as the red line. (a) For a square input profile of 15 ns. (b) For an input profile of 15 ns shaped to pre-compensation saturation. These measurements are made for a total output energy higher than 20 J.

(Figure 5(b)) to reach a nearly flat-top output pulse. This measurement shows that the CBC scheme proposed in this work is fully compatible with the temporal pulse shaping.

One of the key issues concerning efficient coherent combining with large beams is related to the fact that the two split beams might suffer from local differential wavefront errors. In a Sagnac interferometer, it is often claimed that the two counter-propagating beams travel along the exact same optical path, resulting in built-in co-phasing at the output. However, in the case of large-aperture beams, as illustrated in Figure 6(a), the sides of the two counter-propagating beams do not propagate through the same paths in the amplifiers, accumulating potentially a relative lateral dephasing that could impact the CBC efficiency. To investigate this effect,

https://doi.org/10.1017/hpl.2024.84 Published online by Cambridge University Press

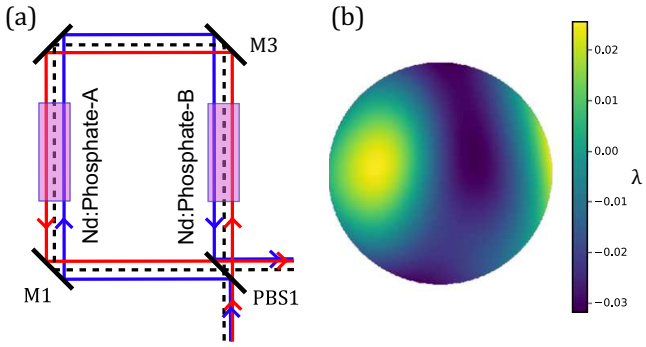

Figure 6. Spatial considerations on the Sagnac interferometer with large beams: (a) optical path of P and S beams; (b) differential wavefront measurement of the two counter-propagating beams in the interferometer.

we measure the local wavefront difference between the two beams using a standard 'shearing' interferometry algorithm. A small angle α is intentionally introduced between the two beams with mirror M2 to obtain a fringe pattern similar to that in Figure 2(a). Using a Fourier transform and filtering in the frequency space, we can reconstruct the differential wavefront (Figure 6(b)). The maximum differential error is approximately equal to $\lambda/20$ peak-to-valley (excluding the tilt and the piston). The impact of this differential phase on the combining efficiency is evaluated to be approximately equal to 1%, validating the CBC for large beams. Moreover, the counter-propagating beams are transversely flipped in the amplifiers, which produce a spatial averaging and smoothing of eventual hotspots.

5. Conclusion

In conclusion, we adapted an existing high-energy laser facility to perform a passive CBC experiment within a Sagnac interferometer configuration. This experiment was set up with minimal modifications to the chain and demonstrated, for the first time to our knowledge, high-energy passive CBC for multi-centimeter beam sizes. We succeeded in combining up to 20 J with an average efficiency of 92%. The results obtained show the compatibility of the examined CBC technique with large-aperture temporally profiled high-energy pulses. In addition, we demonstrated the absence of any significant retro-injection light (<0.1%), guaranteeing the integrity of the laser chain. The results of this experiment pave the way for advancing the scalability of high-energy and high-repetition-rate laser chains. We need to note that in these proof-of-principle CBC experiments we had to respect the operation point of the two Nd:glass amplifiers, limited in the current configuration of the HERA facility to only 10 J, relatively far from saturation (50 J is the estimated stored energy). Our CBC setup, however, could be also applied in the case of deeply saturated amplifiers, as saturation is not expected to have an important impact either on the relative wavefront distortions of the two amplifiers or on the energetic balance of the two counter-propagating beams in the Sagnac interferometer. This experiment unlocked the bottleneck of using high-energy CBC. The advantages over direct amplification are the reduced fluence during the amplification and, therefore, a reduced B-integral by a factor of 2. To maximize the benefits, the Sagnac CBC setup must be designed in relation to the maximum energy that the combination element (PBS1 in our setup) can handle. In our case, it can be estimated around 100 J considering a reasonable laser induced damage threshold of about 7 J/cm^2. Further energy scaling, potentially to the kJ range, could be obtained with the increase of the aperture of the used amplifiers under the condition of high-quality optics to keep the differential wavefront errors of the two counter-propagating beams in the $\lambda/10$ range. The number of amplifiers that could be passively combined based on an interferometer configuration can, in theory, be arbitrarily increased[16], presenting a highly interesting perspective in terms of energy and average power scaling. However, this needs to be carefully investigated in a dedicated study taking into account the increased complexity of the setup and the exact impact of the optical quality of all involved elements. Finally, we note the compatibility of the proposed CBC configuration with large-bandwidth nanosecond pulses or chirped pulse amplification (CPA) systems in the framework of high-intensity PW-class systems[6,12,17,18].

Acknowledgements

This project has received funding from the European Union's HORIZON-INFRA-2022-TECH-01 call under grant agreement number 101095207.

The HERA facility was partially funded by the 'SESAME filières PIA' call for projects from Bpifrance for the 'CRONOS' project, contract numbers DOS0153845/00 and DOS0153842/00.

References

1. H. Abu-Shawareb, R. Acree, P. Adams, *et al.*, Phys. Rev. Lett. **132**, 065102 (2024).
2. A. Azhari, S. Sulaiman, and A. K. Prasada Rao, IOP Conf. Ser.: Mater. Sci. Eng. **114**, 012002 (2016).
3. M. Hanna, F. Guichard, Y. Zaouter, D. N. Papadopoulos, F. Druon, and P. Georges, J. Phys. B: At. Mol. Opt. Phys. **49**, 062004 (2016).
4. Q. Liu, S. Janicot, P. Georges, and G. Lucas-Leclin, Opt. Lett., **48**, 489 (2023).
5. F. Guichard, M. Hanna, Y. Zaouter, D. N. Papadopoulos, F. Druon, and P. Georges, IEEE J. Sel. Top. Quantum Electron. **20**, 619 (2014).
6. D. Papadopoulos, F. Friebel, A. Pellegrina, M. Hanna, P. Camy, J.-L. Doualan, R. Moncorge, F. Druon, and P. Georges, IEEE J. Sel. Top. Quantum Electron. **21**, 3100211 (2014).
7. J. Pouysegur B. Weichelt, F. Guichard Y. Zaouter, C. Hönninger, E. Mottay, F. Druon, and P. Georges, Opt. Express **24**, 9896 (2016).

https://doi.org/10.1017/hpl.2024.84 Published online by Cambridge University Press

8. M. Kienel, M. Müller, S. Demmler, J. Rothhardt, A. Klenke, T. Eidam, J. Limpert, and A. Tünnermann, Opt. Lett. **39**, 3278 (2014).
9. I. Fsaifes, L. Daniault, S. Bellanger, M. Veinhard, J. Bourderionnet, C. Larat, E. Lallier, E. Durand, A. Brignon, and J.-C. Chanteloup, Opt. Express **28**, 20152 (2020).
10. C. Cui, Y. Wang, Z. Lu, H. Yuan, Y. Wang, Y. Chen, Q. Wang, Z. Bai, and R. P. Mildren, Opt. Express **26**, 32717 (2018).
11. R. Kirkwood, D. Turnbull, T. Chapman, S. Wilks, M. Rosen, R. London, L. Pickworth, A. Colaitis, W. Dunlop, P. Poole, J. Moody, D. Strozzi, P. Michel, L. Divol, O. Landen, B. MacGowan, B. Wonterghem, K. Fournier, and B. Blue, Phys. Plasmas **25**, 056701 (2018).
12. H. J. Kong, S. Park, S. Cha, H. Ahn, H. Lee, J. Oh, B. J. Lee, S. Choi, and J. S. Kim, High Power Laser Sci. Eng. **3**, e1 (2015).
13. R. Humblot, L. Meignien, F. Druon, and P. Audebert, in *High-Brightness Sources and Light-Driven Interactions Congress* (2024), paper JTu4A.22.
14. S. Roither, A. J. Verhoef, O. D. Mücke, G. A. Reider, A. Pugžlys, and A. Baltuška, Opt. Express **20**, 25121 (2012).
15. R. Humblot, J. D. Sousa, C. Rapeneau, S. Baton, P. Audebert, F. Druon, and L. Meignien, Opt. Express **32**, 37959 (2024).
16. D. Papadopoulos, M. Hanna, and L. Daniault, "Passive device and method for the coherent combination of a plurality of optical amplifiers," Patent US9042009B2 (26 May, 2015).
17. D. Wang and Y. Leng, Opt. Express **27**, 36137 (2019).
18. F. Guichard, Y. Zaouter, M. Hanna, K.-L. Mai, F. Morin, C. Hönninger, E. Mottay, and P. Georges, Opt. Lett. **40**, 89 (2015).

https://doi.org/10.1017/hpl.2024.84 Published online by Cambridge University Press